PHILOSOPHICAL TRANSACTIONS OF THE ROYAL SOCIETY B BIOLOGICAL SCIENCES

Ontogenetic Changes in the Skull of the Carboniferous Tetrapod Greererpeton burkemorani Romer, 1969

S. J. Godfrey

Phil. Trans. R. Soc. Lond. B 1989 **323**, 135-153
doi: 10.1098/rstb.1989.0003

Phil. Trans. R. Soc. Lond. B **323**, 135–153 (1989) [135]
Printed in Great Britain

ONTOGENETIC CHANGES IN THE SKULL OF THE CARBONIFEROUS TETRAPOD *GREERERPETON BURKEMORANI* ROMER, 1969

BY S. J. GODFREY

Redpath Museum, McGill University, 859 Sherbrooke Street West, Montreal, Quebec, Canada H3A 2K6

(*Communicated by H. B. Whittington, F.R.S.* – *Received* 16 *July* 1987 – *Revised* 15 *February* 1988)

A partial growth series, representing a 4.4-fold increase in the linear dimensions of the skull of *Greererpeton burkemorani* Romer, 1969, reveals that allometric changes are limited to: (1) an increase in the area of some circumorbital bones (primarily the lacrimal, jugal, and postorbital); (2) a small increase in the width of the skull table across the tabulars; (3) a decrease in the length and an increase in the width of the braincase relative to skull length; and (4) an anteromesial shift in the stapedial foot plate relative to its distal flattened plate. The position of the orbits does not appear to shift posteriorly over the growth interval studied. As the proportions of the braincase change relative to the remainder of the skull during ontogeny, so too do the proportions of the stapes for it to maintain its role as one of the principle supports for the back of the braincase.

INTRODUCTION

In a study of ontogenetic changes in the Devonian osteolepiform fish *Eusthenopteron foordi*, Schultze (1984) noted that although growth cannot be studied directly from fossils, a size series may be interpreted as a growth series if the fossils belong to one species and are derived from a deposit representing a short time interval. The well-preserved fossils of *Greererpeton burkemorani* Romer, 1969, from the Bluefield Formation at Greer, West Virginia, appear to satisfy these

conditions. Remains of approximately 60 individuals of this species were collected between 1968 and 1973 by the Cleveland Museum of Natural History from a bone bed containing a nearly solid mass of fish and amphibian remains (Godfrey 1988, 1989).

Most species of Carboniferous amphibians are known from relatively few fossils. If more than one specimen is known for any given taxon, the sample is usually biased or skewed, representing a relatively small portion of their total growth range. Because growth series of Carboniferous tetrapods are few and far between, the 4.4-fold increase in the linear dimensions of the known material of *G. burkemorani* provides a rare opportunity to document alterations that occur in its cranial proportions during ontogeny.

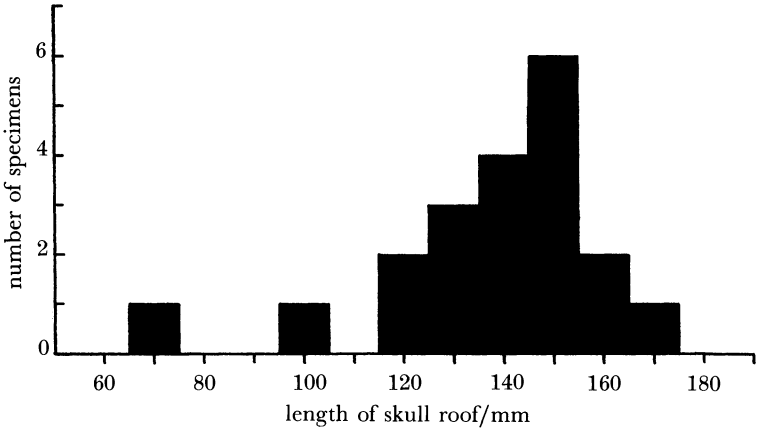

FIGURE 1. Histogram showing the distribution of skull length in 20 specimens of *Greererpeton burkemorani* Romer.

MATERIALS AND METHODS

Over twenty skulls of *G. burkemorani* (varying in degree of completeness) are known. Although most skulls are between 120 and 160 mm long (snout–postparietal length) (figure 1), several specimens (figures 2 and 3) are much smaller. Because the degree of sexual maturity cannot be determined on the basis of the skeletal remains of *G. burkemorani*, the terms juvenile and subadult will be based arbitrarily on absolute size. I shall adopt, for this study, the definition of juvenile, or subadult, as individuals with a snout–postparietal length (measured along the midline) no greater than 135 mm (less than 80% of the length of the largest known skull).

The following analysis of ontogenetic changes in the skull of *G. burkemorani* will be divided into two major, but overlapping, sections. The first section describes relative growth in the skull by using principal-component analysis based on the variance–covariance matrix. The second section considers ontogenetic changes, primarily in the braincase and stapes, in a more traditional fashion: the shape of component elements, how they co-ossify, and the changing pattern of foramina or grooves for vascular and/or nervous tissue, for example.

Principal-component analysis (PCA) a multivariate analysis technique, reduces a large number of correlated variables to some smaller number of underlying variates that one hopes to identify. Many authors (Jolicoeur & Mosimann 1960; Jolicoeur 1963; Blackith & Reyment 1971; Dodson 1975*a*; Chatfield & Collins 1980; Gould 1975, 1981) have provided lucid explanations of the principles behind this technique. Blackith & Reyment (1971) have reviewed many examples of its application.

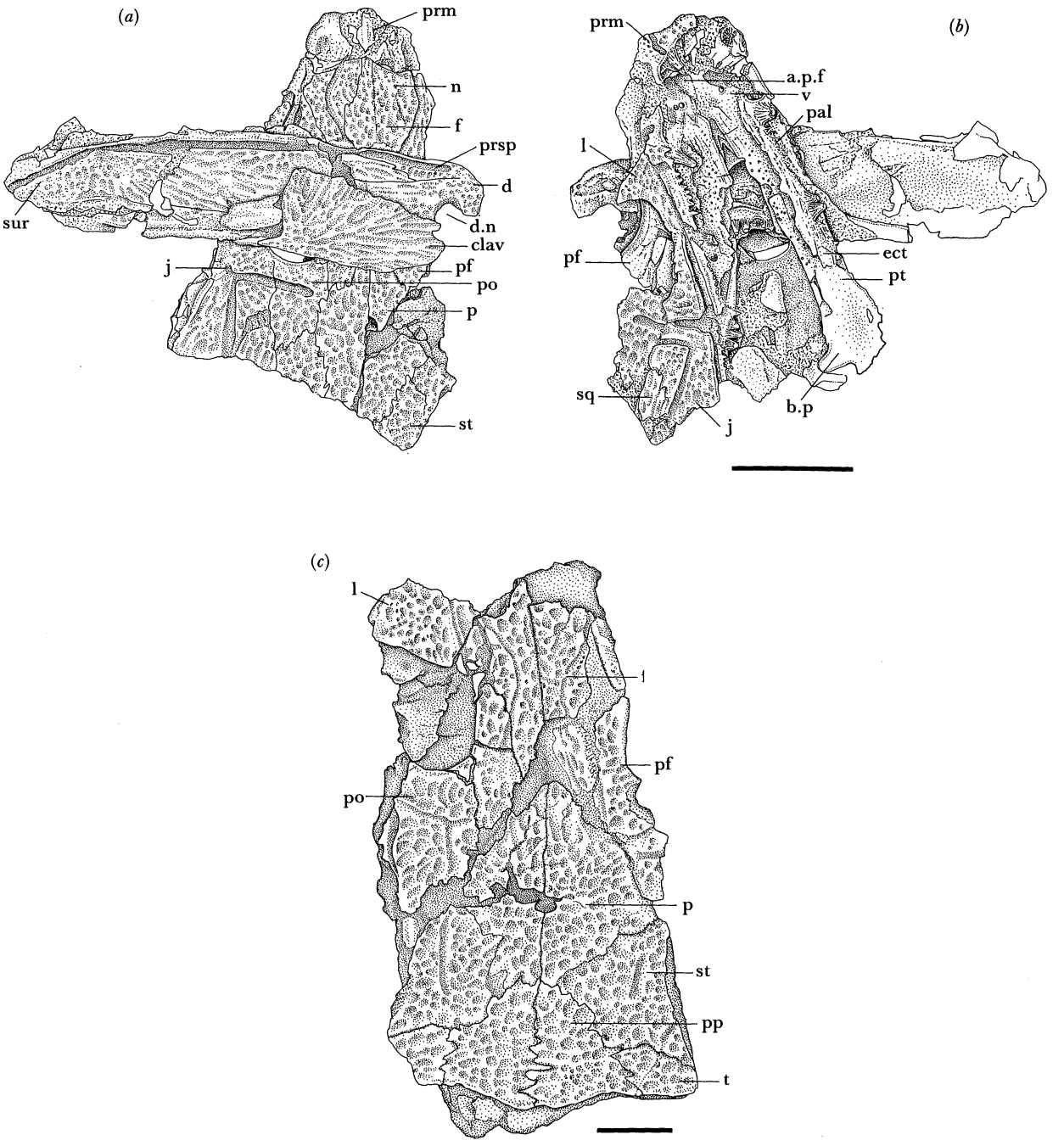

FIGURE 2. *Greererpeton burkemorani* Romer. (*a*, *b*), CMNH 11095. Partial cranium, left mandible and clavicle of the smallest known individual in dorsal and ventral views respectively. (*c*) CMNH 11113, an incomplete skull of a subadult in dorsal view. Scale bars 1 cm.

The first principal component is the axis that best describes the trend of the cluster of observations in multidimensional space (i.e. resolves the maximum amount of variance). The second principal component describes the next most prominent axis, by convention perpendicular (orthogonal) to, and therefore independent of, the first, thus absorbing the maximum amount of residual variance (Dodson 1975*a*). Successive principal components

account for the remaining variance (Blackith & Reyment 1971). Eigenvalues, usually expressed as a percentage of the total variance, describe the amount of information resolved by each component. In a multivariate analysis where a large growth series exists, the first principal component usually accounts for more than 90% of the total variance. Jolicoeur & Mosimann (1960) and others have shown that the first principal component often has the character of a size vector. Under these circumstances they emphasize that all coefficients of the first vector must be of the same sign, whereas those of subsequent components must generally have mixed signs for this interpretation to be valid. The sign and magnitude of each eigenvector coefficient indicates the direction (sign) and importance of the contribution of the particular variable to the given component. Factor loadings of low magnitude contribute little to the particular component and are ignored.

Principal-component analysis was done by using the Statistical Analysis System (SAS Institute 1982) principal-component program. The program deletes all the data for a specimen if one or more values are missing. For that reason, different combinations of variables were grouped together to maximize the number of observations per analysis (see table 1).

To evaluate the pattern of relative growth in the skull of *G. burkemorani*, the following measurements were taken from 20 individuals (Appendix 1; the letters *A*–*L* correspond to those in figure A 1):

A: length of the skull from the anterior margin of the premaxilla to the posterior margin of the postparietal (snout–postparietal length = skull length);

B: snout–pineal length;

C: pineal–postparietal length;

D: snout–midorbital length;

E: distance between the orbits;

F: maximum orbital length;

G: minimum height of the jugal between the maxilla and the orbital margin;

H: skull width across the tabulars;

I: length of the braincase from the transverse line through the basipterygoid processes to the posterior margin of the basioccipital (or parasphenoid);

J: width of the braincase across the basipterygoid processes;

K: anteroposterior length of the stapes;

L: mesiolateral width of the stapes.

Description

The skull

Smithson's (1982) description of the adult cranial morphology of *G. burkemorani* will not be repeated here. Nevertheless, in an attempt to set the stage for a description of juvenile cranial morphology, a brief synopsis of the adult anatomy is relevant.

In dorsal view, the skull is narrow anteriorly but expands gradually towards the region of the adductor chambers (see figure 4*d*). The skull is conspicuously compressed dorsoventrally (see figure 4*b*) such that the depth of the lower jaw almost equals the height of the skull. The orbits are essentially oval and lie approximately midway between the snout and occiput. In large individuals, the orbits face almost entirely dorsally and are barely visible in lateral view. A small pineal opening lies approximately midway between the posterior margin of the orbits

and the postparietals. The suspensorium projects little beyond the occiput and the lower jaw does not develop a retroarticular process. The external surface of the dermal bone is ornamented with a honeycomb pattern of fairly deep pits and/or grooves.

The results of the principal-component analyses on the skull of *G. burkemorani* are given in table 1. Only the first three principal components (Prin 1–Prin 3 of table 1) of each analysis are included in this table as they account for no less than 98% of the total variance.

Several general trends are seen to occur throughout. Of the total variance in each analysis, the first principal component always accounts for more than 93% (range from about 93% to more than 98%). This tight clustering of the vectors is not surprising, as a strong correlation between growing skull parts is due primarily to an overall increase in skull size.

If all the variables measured within the skull of *G. burkemorani* increased in size without any corresponding change in proportion, then the coefficients of the first principal component would all be equal and no variance would remain. A close examination of the first eigenvector coefficients in any analysis shows which variables changed isometrically and which did not. From these coefficients it appears that most of the cranium grew isometrically throughout the growth interval represented by the material (table 1). In the first analysis (table 1*a*), for example, skull length, snout–pineal length, pineal–postparietal length and the distance between the orbits have approximately equal coefficients (Prin 1: 0.315–0.346). These are interpreted as variables that changed isometrically with respect to an overall increase in skull size.

The most conspicuous allometric change in the dermal skull roof was a relative decrease in orbit diameter with positive allometry of several (lacrimal, jugal, and postorbital), but not all, circumorbital bones (see figure 4). In those analyses that include orbital length, it is always the smallest coefficient, indicating that although the diameter actually increased during ontogeny it did so at a much slower rate as compared with other cranial dimensions. The large orbits in CMNH 11095 (figures 2*a*, *b* and 4*a*, *c*) face dorsolaterally with their ventrolateral margin just precluded from making contact with the maxilla by the union of stiletto-like strips of bone from the lacrimal and jugal. During ontogeny, the transverse distance between the mesial margins of the orbits changed isometrically relative to skull length. Therefore, to attain the adult configuration, in which the orbits are directed almost entirely dorsally, both the lacrimal and jugal grew rapidly in a dorsomesial direction. The lateral restorations of CMNH 11095 and CMNH 11068 (figure 4) illustrate the close correlation between the relative decrease in orbit diameter and the disproportionate increase in the area of these two elements. The minimum height of the jugal below the orbit was measured to gauge how circumorbital parameters changed relative to other cranial dimensions. In those analyses that include this variable it always exhibits the largest coefficient projection, confirming that this area had the highest growth rate of dermal bone over the ontogenetic interval.

The only other proportional change noted in the dermal roof was a positive allometric increase in the width of the skull table across the tabulars. The first principal component coefficient for this variable is always larger than the coefficient for skull length. In adults, the lateral edges of the small rhomboidal tabulars are normally firmly sutured to the squamosal, eliminating the primitive kinetic margin between the skull table and cheek (Smithson 1982). In the smallest skull that preserves the posterior border of the skull table and cheek (CMNH 11320, figure 3), a conspicuous discontinuity exists between these areas. Although this discontinuity probably does not represent the retention of a functional lateral kinesis, it was

PHILOSOPHICAL TRANSACTIONS OF THE ROYAL SOCIETY B BIOLOGICAL SCIENCES

TABLE 1. ABRIDGED RESULTS OF SEVERAL PRINCIPAL-COMPONENT ANALYSES ON THE SKULL OF *GREERERPETON BURKEMORANI* ROMER

(*a*) 10 observations, 8 variables

	Prin1	Prin2	Prin3
skull length (snout–postparietal)	0.332	0.227	−0.010
snout–pineal length	0.340	0.189	−0.010
pineal–postparietal length	0.315	0.271	0.171
distance between the orbits	0.346	−0.099	0.232
maximum orbital length	0.226	0.368	0.062
minimum height of the jugal	0.497	−0.591	−0.590
skull width across the tabulars	0.438	−0.257	0.603
braincase length	0.252	0.527	−0.446
proportion of the total variance	0.9556	0.0187	0.009
cumulative proportion of variance	0.9556	0.9744	0.984

(*b*) 16 observations, 4 variables

	Prin1	Prin2	Prin3
skull length (snout–postparietal)	0.425	0.310	0.413
pineal–postparietal length	0.411	0.543	0.336
minimum height of the jugal	0.593	−0.760	0.221
skull width across the tabulars	0.546	0.175	−0.816
proportion of the total variance	0.9506	0.0320	0.014
cumulative proportion of variance	0.9506	0.9826	0.996

(*c*) 8 observations, 7 variables

	Prin1	Prin2	Prin3
skull length (snout–postparietal)	0.278	0.082	0.275
snout–midorbital length	0.263	0.344	0.528
skull width across the tabulars	0.382	−0.562	−0.033
braincase length	0.223	0.613	−0.380
braincase width	0.338	0.249	−0.509
stapes anteroposterior length	0.453	0.141	0.426
stapes mesiolateral width	0.580	−0.317	−0.240
proportion of the total variance	0.9825	0.0093	0.005
cumulative proportion of variance	0.9825	0.9918	0.997

(*d*) 15 observations, 4 variables

	Prin1	Prin2	Prin3
snout–pineal length	0.407	0.426	0.617
distance between the orbits	0.400	0.477	−0.757
maximum orbital length	0.292	0.425	0.212
minimum height of the jugal	0.766	−0.639	−0.012
proportion of the total variance	0.9816	0.0115	0.004
cumulative proportion of variance	0.9816	0.9931	0.997

(*e*) 14 observations, 7 variables

	Prin1	Prin2	Prin3
skull length (snout–postparietal)	0.351	0.257	−0.170
snout–pineal length	0.360	0.307	−0.158
pineal–postparietal length	0.345	0.498	−0.290
distance between the orbits	0.345	−0.196	0.695
maximum orbital length	0.231	0.255	0.275
minimum height of the jugal	0.498	−0.696	−0.454
skull width across the tabulars	0.453	−0.038	0.309
proportion of the total variance	0.9329	0.0292	0.020
cumulative proportion of variance	0.9329	0.9621	0.982

(*f*) 14 observations, 6 variables

	Prin1	Prin2	Prin3
skull length (snout–postparietal)	0.360	0.288	−0.136
snout–pineal length	0.370	0.334	−0.123
pineal–postparietal length	0.354	0.565	−0.166
distance between the orbits	0.354	−0.271	0.657
minimum height of the jugal	0.513	−0.641	−0.556
skull width across the tabulars	0.446	−0.007	0.443
proportion of the total variance	0.9396	0.0297	0.020
cumulative proportion of variance	0.9396	0.9694	0.989

PHILOSOPHICAL TRANSACTIONS OF THE ROYAL SOCIETY B BIOLOGICAL SCIENCES

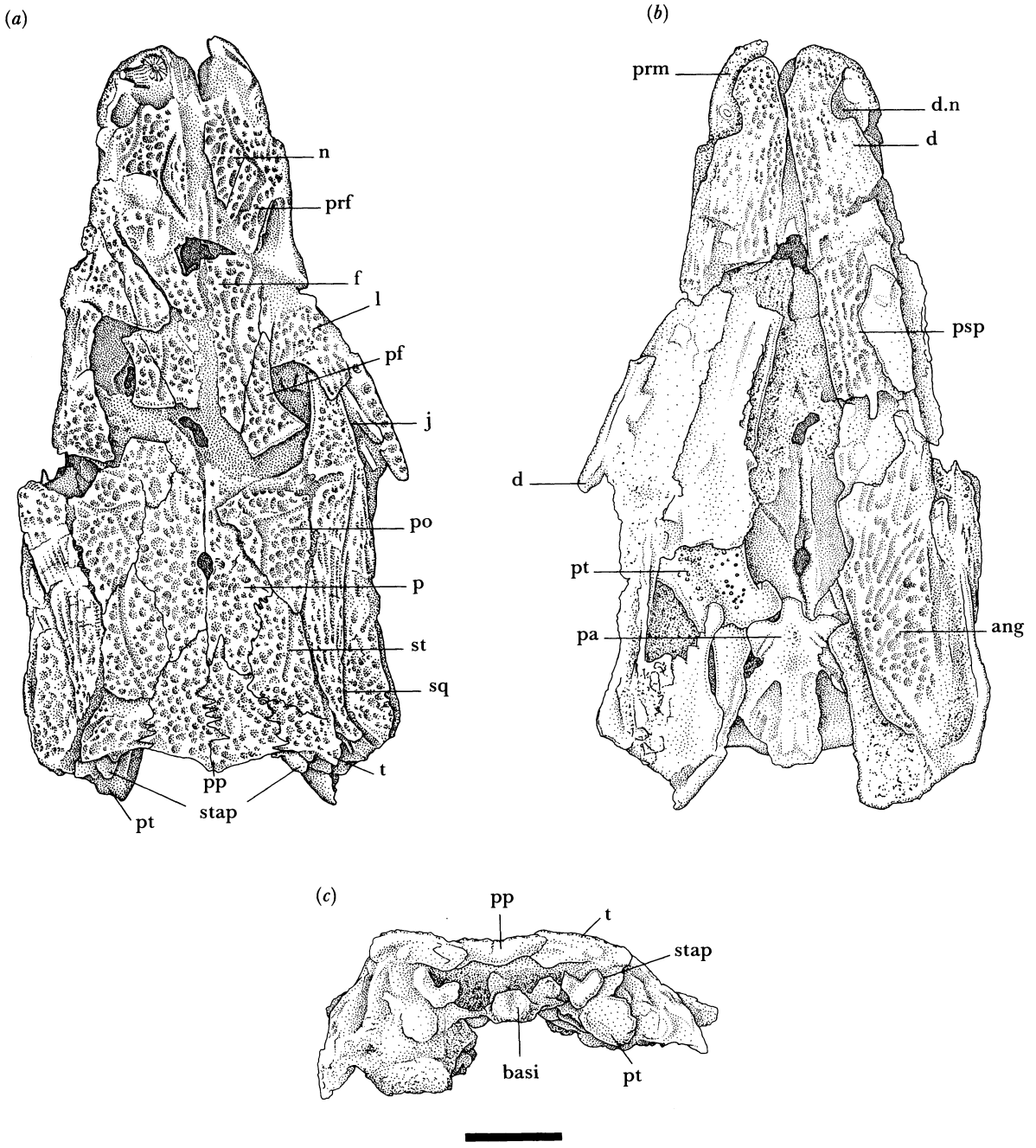

FIGURE 3. *Greererpeton burkemorani* Romer, CMNH 11320. The skull of a juvenile in (*a*) dorsal view, (*b*) ventral view and (*c*) occipital view. Scale bar 1 cm.

a definite line of weakness, which was eliminated during ontogeny. In subadult specimens that suffered moderate degrees of crushing *post mortem*, the cheeks are often splayed away from the skull table. In progressively larger individuals, this parasagittal line of weakness is interrupted by the increasing width of the posterior margin of the skull table. In some specimens, the 'kinetic' margin is further interrupted by an anteromesial flange of the squamosal, deeply embedded between the postorbital and supratemporal (figure 4*d*). The largest skulls showing crushing *post mortem* are rarely disrupted preferentially along this former line of weakness.

PHILOSOPHICAL TRANSACTIONS OF THE ROYAL SOCIETY B BIOLOGICAL SCIENCES

In a partial growth series illustrating the latter part of ontogeny, Smithson (1982, figure 8) shows snout–midorbital growth to be positively allometric. A careful study of the specimens (table 1*c*) indicates that snout–midorbital length increased at virtually the same rate as did skull length. In *G. burkemorani* the distance from the snout to the anterior margin of the orbits did become progressively longer during ontogeny, however. This increase did not result from an elongation of the snout, but rather from the proportional decrease in the diameter of the orbits (*contra* Smithson 1982).

Because the lateral margins of the palate are obscured by the underlying mandibles in most specimens, no attempt was made to document allometric changes in this area.

The braincase

During ontogeny the length of the braincase decreased, but not greatly so, relative to the overall length of the skull (table 1*c*). On the other hand, the width of the braincase across the basipterygoid processes grew at a faster rate than did the length of the skull. These trends are apparent in the growth series presented in figure 5. When the width of the braincase is compared with the allometric increase in the width of the skull table across the tabulars, the width of the braincase does not appear to have grown as fast.

The braincase of the juvenile, CMNH 11320 (figure 5*a*), is about half the length of those used by Smithson (1982) to detail its anatomy (CMNH 11319, CMNH 11079 and CMNH 11090). As in adults, the basipterygoid processes, the parasphenoid, and the basisphenoid are co-ossified in subadults. A small patch of denticles lies between the basipterygoid processes on the ventral surface of the parasphenoid in CMNH 11320. However, they are not nearly as well developed as in mature individuals. A noteworthy difference between the ventral surface of the parasphenoid in CMNH 11320 and adults is the presence of four conspicuous grooves in the former, a pair around the posteromesial base of each basipterygoid process. Each groove lies parallel to its mate and they may have held the internal carotid artery and palatine vein in life (Shishkin 1968). Smithson (1982) noted the absence of these grooves in *G. burkemorani*. It is difficult to know whether they vanish during ontogeny or were inadvertently removed during preparation.

Behind the basipterygoid process in CMNH 11320, the braincase narrows but proportionately not as much as one might expect from examining larger, but not fully mature, individuals. As Smithson (1982) has shown, fully mature specimens possess a more completely ossified basisphenoid, extending above the parasphenoid to contact the pro-otic. In immature individuals, there is a distinct division between the dorsum sellae and the otic capsule because the basisphenoid remains unossified between the two areas. In the largest braincases, the basisphenoid is ossified and slants dorsolaterally such that the foramen that probably transmitted the principal ramus of the facial nerve (VII) is visible in ventral view, immediately behind the basispterygoid processes (figure 5*f*, *h*). Immediately behind the oval patch of denticles in CMNH 11320 is a conspicuous concavity. This feature is present in adults, but greatly reduced.

Behind the 'waisted' region of the braincase, the parasphenoid in CMNH 11320 expands to form two lateral flanges, the cristae ventrolaterales. These flanges extend just beyond the level of the basipterygoid processes and are remarkably well ossified in this small individual. Posteriorly they form the ventral border of the fenestrae ovales. In adults, the cristae ventrolaterales are distinct lateral flanges of the parasphenoid. In CMNH 11320, by contrast,

PHILOSOPHICAL TRANSACTIONS OF THE ROYAL SOCIETY B BIOLOGICAL SCIENCES

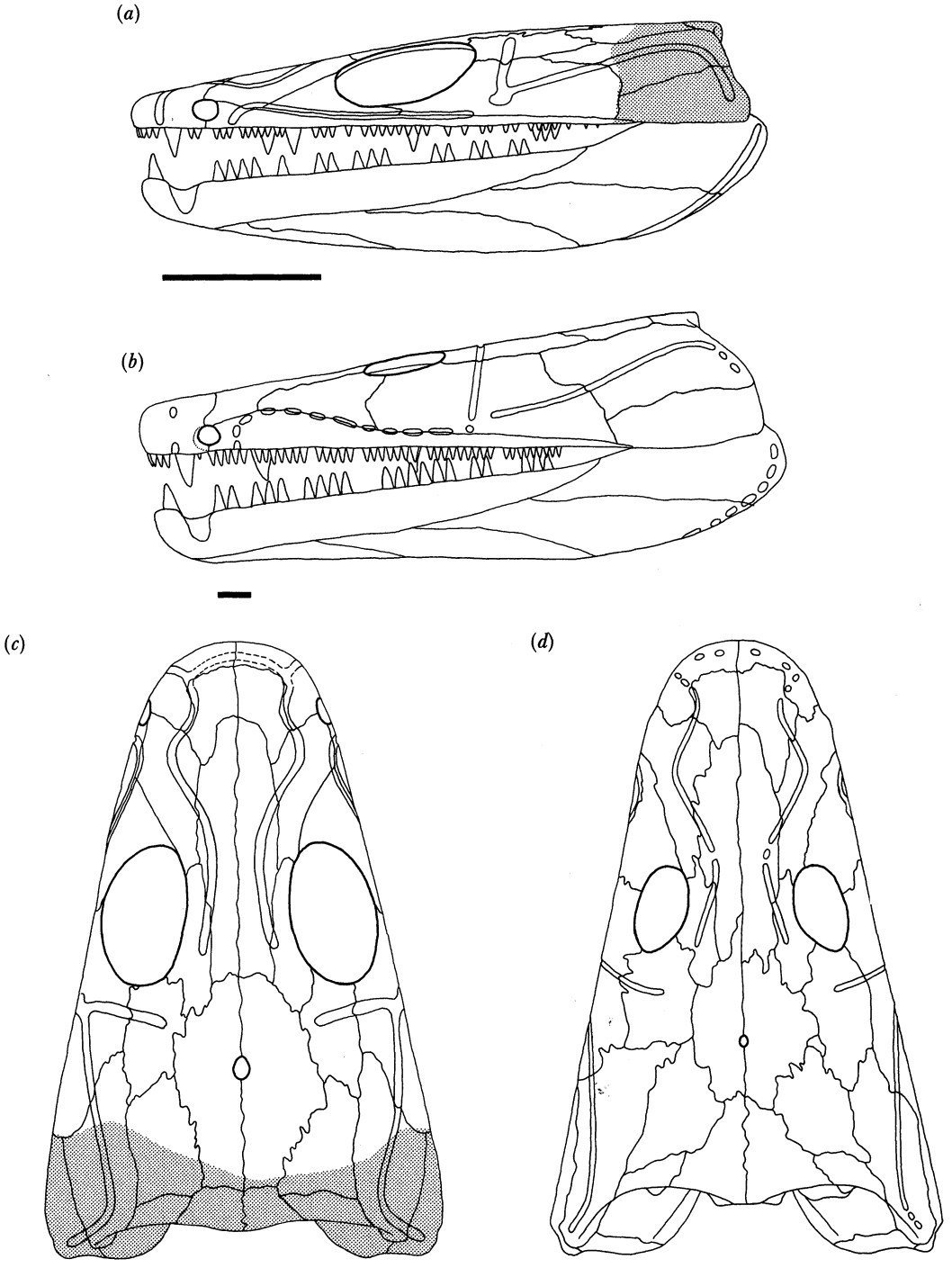

FIGURE 4. *Greererpeton burkemorani* Romer: changes in cranial proportions during ontogeny. (*a*, *c*) Restorations based on CMNH 11095; (*b*, *d*) restorations based on CMNH 11068 (redrawn from Smithson (1982)). (*a*, *b*) Left lateral views; (*c*, *d*) dorsal views. Both skulls were drawn to the same length to facilitate comparison. The shaded area in CMNH 11095 is not preserved in the specimen (see figure 2). Scale bars 1 cm.

PHILOSOPHICAL TRANSACTIONS OF THE ROYAL SOCIETY B BIOLOGICAL SCIENCES

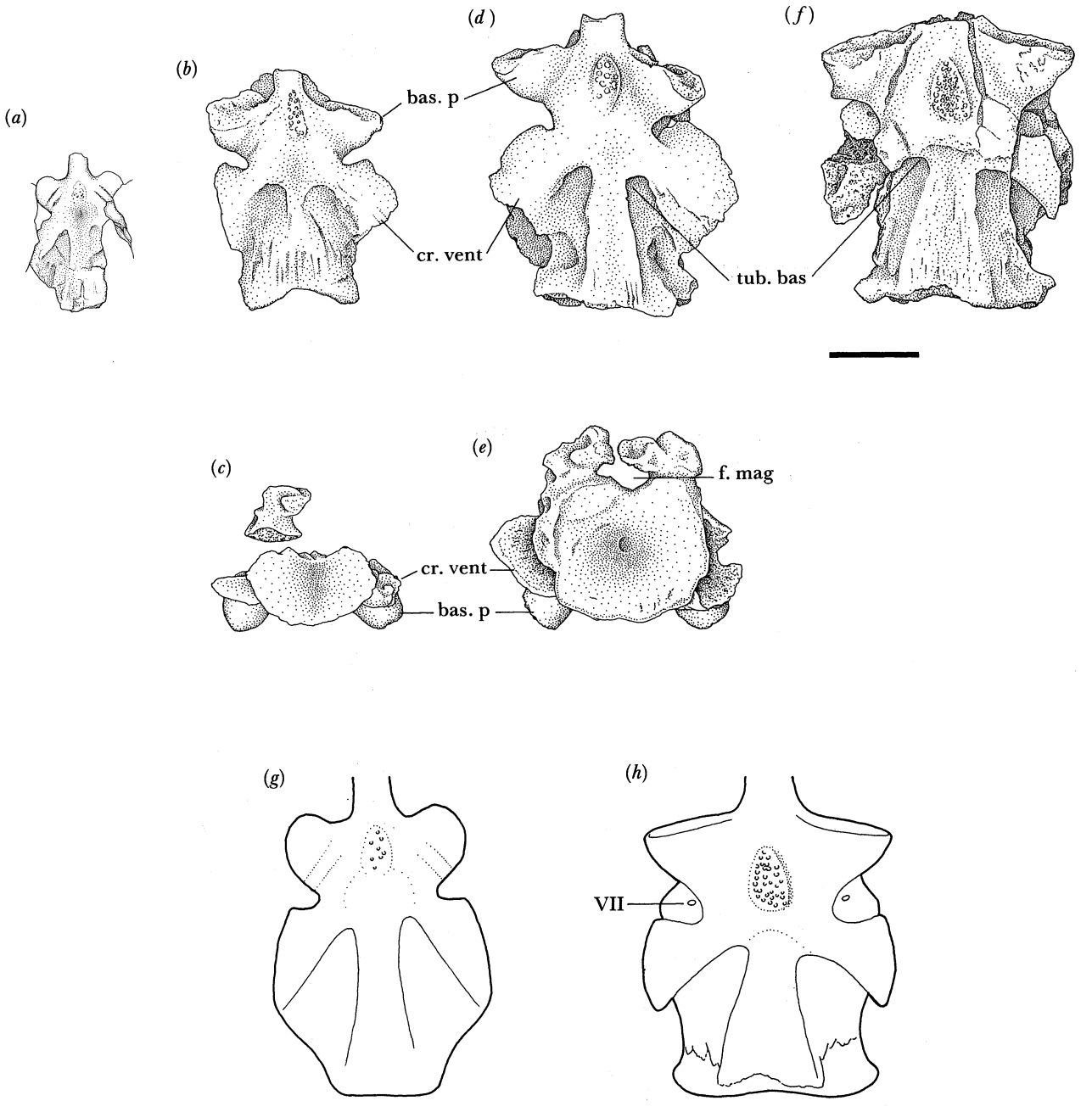

FIGURE 5. *Greererpeton burkemorani* Romer: changes to the braincase during ontogeny. (*a*) CMNH 11320; (*b*, *c*) CMNH 11231; (*d*, *e*) CMNH 11079; (*f*) CMNH 11319. (*a*, *b*, *d*, *f*) Ventral view; (*c*, *d*) posterior (occipital) view. (*g*, *h*) Restorations of the braincase after CMNH 11320 and 11319 respectively. Scale bars 1 cm.

they are essentially confluent with the parasphenoid forming the posterolateral margin of the 'tubera basisphenoidales'.

The 'tubera basisphenoidales' (Romer 1930; two inverted U- or V-shaped depressions on the ventral surface of the parasphenoid) are much less distinct in this specimen than in an adult. Between the 'tubera basisphenoidales', the parasphenoid extends posteriorly as a broad ridge

that underlies the basioccipital. It is evident from examining a number of immature individuals that this ridge became progressively more pronounced during ontogeny. In adults, the parasphenoid extends dorsally along its posterolateral margins to fuse with the ventrolateral rim of the basioccipital. In juveniles, however, the posterolateral borders of the parasphenoid are only mildly concave (in ventral view) and do not fuse with the lateral margins of the incipient basioccipital.

Most of the dorsal surface of the braincase in CMNH 11320 is either obscured because of its close proximity to the dermal skull roof, or incompletely ossified.

The components of the occipital arch in *G. burkemorani* are co-ossified in adults, but several subadults (CMNH 11320 and CMNH 11132) present the basioccipital and the exoccipitals as separate entities. In CMNH 11320, the basioccipital is significantly different from that seen in adults. It rests on the parasphenoid as a distinct element. As in *Edops* (Romer & Witter 1942), the basioccipital in this immature individual is held to the parasphenoid by a system of interlocking parallel ridges and grooves. These ridges and grooves may be seen on the dorsal surface of the parasphenoid anterior and lateral to the basioccipital. The basioccipital pinches out posteriorly to coincide with the posterior margin of the parasphenoid. In posterior view, the basioccipital is ovoid in outline (figure 5*c*). There are no facets on its dorsal surface to indicate where the exoccipitals rested. This area may have been entirely cartilaginous in life. In dorsal aspect, the basioccipital is triangular with its apex directed anteriorly. The lateral and anterior margins are quite distinct from the parasphenoid. In lateral view, the basioccipital is very similar in outline to that of *Edops* (Romer & Witter 1942, figure 10) and *Eryops* (Sawin 1941, plate 10*b*). In this view, the angle formed by the parasphenoid and the median groove running along the posterodorsal surface of the basioccipital is approximately 30°. In mature individuals, the aforementioned angle is between 60° and 70°. In juveniles, the notochord pierced the back of the braincase, extending forward as much as one third of the otico-occipital length. During ontogeny, however, the notochordal entrance into the braincase was progressively restricted by additional ossification of the basioccipital dorsally and the co-ossification or fusion of the exoccipitals to the basioccipital.

In CMNH 11132, a subadult, the exoccipitals are not fused to the basioccipital. In posterior view, the basioccipital is oval, dorsoventrally compressed and concave. In dorsal view, the outline of the anterior margin of the basioccipital is seen on the parasphenoid. The most notable difference between CMNH 11320 and CMNH 11132 is the growth of the posterolateral margin of the basioccipital, from a wedge in the former to a subcircular funnel in the latter. With the growth of the basioccipital dorsally, facets are present in CMNH 11132 to accommodate the pedicels of the exoccipitals. In dorsal view, two ridges sweep anteromesially from the posterodorsal margins of the basioccipital to merge medially. Each ridge runs anteriorly and may be seen in adult specimens (Smithson 1982, figures 15*a* and 16*e*), only partly concealed by the ventral rim of the foramen magnum. On the anterolateral margin of each ridge is a dorsally directed tubercle. This tubercle and the posterior surfaces of the ridges are the sites where the exoccipitals attach to the basioccipital.

The fortuitous preservation of the occipital arch in CMNH 11132 helps establish which arch elements surround the foramen magnum in large individuals in which the basioccipital and exoccipitals are fully co-ossified. In CMNH 11132, the exoccipitals form the lateral and dorsolateral walls of the foramen, and send ventromesial extensions to form its floor, as in *Edops* (Romer & Witter 1942). In no specimen is the foramen enclosed dorsally as in *Eryops* (Sawin

PHILOSOPHICAL TRANSACTIONS OF THE ROYAL SOCIETY B BIOLOGICAL SCIENCES

1941). In CMNH 11132 and CMNH 11079, however, mesially directed flanges on the exoccipitals come close to enclosing the foramen dorsally and probably did so with cartilage in life. This may have been a variable feature, with the postparietals enclosing the foramen dorsally in other individuals (Smithson 1982).

In CMNH 11132, the pedicels of the exoccipitals are characterized by large, essentially circular facets. It is evident from their flat to convex surface that cartilage filled the area between basioccipital and exoccipitals. In lateral view, the exoccipitals are roughly wedge-shaped with the apex of the wedge directed anteroventrally (figure 6*a*, *b*). Piercing the concave mesial surface of the exoccipitals are two foramina. The posterior foramen probably transmitted the major branch of the hypoglossal nerve (XII). The anterior foramen is somewhat smaller; it probably carried a smaller branch of the hypoglossal nerve, as in *Eryops* (Sawin 1941, plate 7*b*). In CMNH 11132 and CMNH 11231, the route of the anterior hypoglossal foramen is seen in lateral view. A short distance behind its lateral emergence it bifurcates to form a Y-shaped groove. The base of the Y is directed anteriorly, with both posterolateral branches coming very close to the lateral opening of the more posterior branch of the hypoglossal nerve.

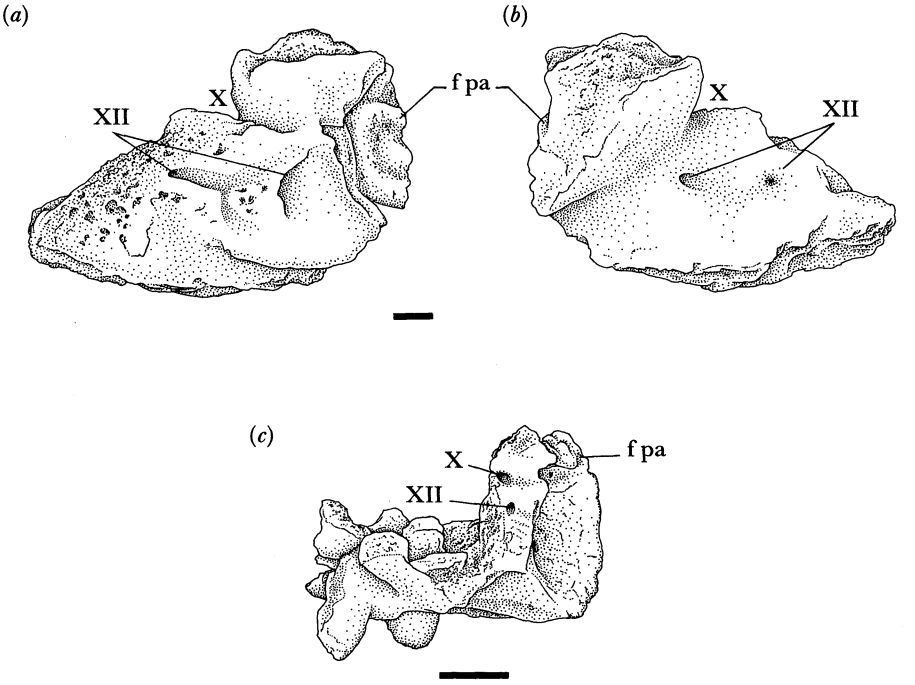

FIGURE 6. *Greererpeton burkemorani* Romer. (*a*) The left exoccipital of CMNH 11231 in lateral view showing the course of cranial nerves X and XII; (*b*) mesial view. (*c*) An oblique posterolateral view of the braincase of CMNH 11079 showing the position of the foramina for cranial nerves X and XII. (*a*, *b*) Scale bar 1 mm; (*c*) scale bar 1 cm.

The stapes

Following the description of the adult stapes of *G. burkemorani* by Smithson (1982), an unprepared skull of a juvenile was discovered in the collection of material from the Cleveland Museum of Natural History. The occiput had suffered very little *post mortem* distortion and careful preparation revealed that both stapes were preserved in a lifelike position, lying against

the quadrate ramus of the pterygoid (figure 3*c*). The right stapes was removed to facilitate its description.

The stapes of CMNH 11320, like that in adult specimens, is expanded proximally, constricted immediately lateral to the foot plate (but less so than in adults), and flattened distally (figure 7*a–d*). Viewed mesially (figure 7*c*), the foot plate is square to rectangular in outline, not circular as in adults. Its mesial surface is unfinished and was probably covered by a large cartilaginous cap in life. A striking feature of the juvenile stapes is the large size of the foot plate relative to the size of the distal flattened plate. The proximal surface area of the former is roughly equivalent to the ventral surface area of the latter. In adults (figure 8), the ventral surface area of the distal flattened plate is more than twice as large as the mesial surface area of the stapedial head. Precocious ossification of the stapedial head in *G. burkemorani* may be a result of the relatively large minimum size of otic capsules in juvenile amphibians (Bernacsek & Carroll 1981).

Immediately lateral to the head of the stapes in adults, the bone is deeply notched. This notch probably marks the course of the vena capitis lateralis and the ramus mandibularis of the facial nerve (VII) (chorda tympani). In contrast, no groove appears on the posterodorsal surface of the distal flattened plate to convey these vessels in CMNH 11320. This shallow groove presumably developed later in ontogeny as the flattened plate increased in size. It should be noted, however, that the depth of the groove does vary somewhat in adults. In CMNH 11231, the usually shallow groove has become deeply embedded within the body of the distal flattened plate (figure 7*e–g*). Immediately below and lateral to the stapedial head the bone has overgrown the groove, so that it is almost enclosed dorsally to form a second 'stapedial' foramen. In anterior view, it appears as though the trough that may have conveyed the vena capitis lateralis and the ramus mandibularis either entered the body of the stapes together with the stapedial artery or passed immediately above it. The development of a deep trough is unique to this specimen but confirms that the shallow groove seen in other specimens probably conveyed vascular tissue, nervous tissue, or both.

One of the most notable differences between the juvenile and adult stapes is the position of the stapedial foramen relative to the stapedial head and plate (figure 8). In an antero-dorsolateral view of the stapes of CMNH 11320 (figure 8*a*), a small dorsally directed thumb-like flange of bone would have just 'captured' the stapedial artery and incorporated it into the head of the ossicle. The dorsal and ventral projections of bone forming the anteromesial rim of the foramen had not, however, fused. In both juveniles and adults, this foramen passes anterolaterally through the stapes. However, when the stapes is viewed from above, perpendicular to the plane of the distal flattened plate, a straight line passing through the foramen lies posterolateral to the proximal stapedial head in adults, whereas in CMNH 11320 it passes below the main ossified portion of the head. The apparent posterolateral movement of the stapedial artery during ontogeny was the result of progressive ossification of the stapedial head mesially. The ontogenetic series illustrated in figure 8 demonstrates that the stapedial artery was surrounded by the body of the bone during ontogeny, as in extant vertebrates (de Beer 1937).

In figure 8*f–h*, each stapes was drawn with the ventrolateral portion of the distal flattened plate perpendicular to the viewer. In CMNH 11320, the head is bisected by an extension of the line formed by the anterior margin of the flattened plate such that the length of *a* (*a* = anterior) equals the length of *p* (*p* = posterior). During ontogeny, there was a progressive

PHILOSOPHICAL TRANSACTIONS OF THE ROYAL SOCIETY B BIOLOGICAL SCIENCES

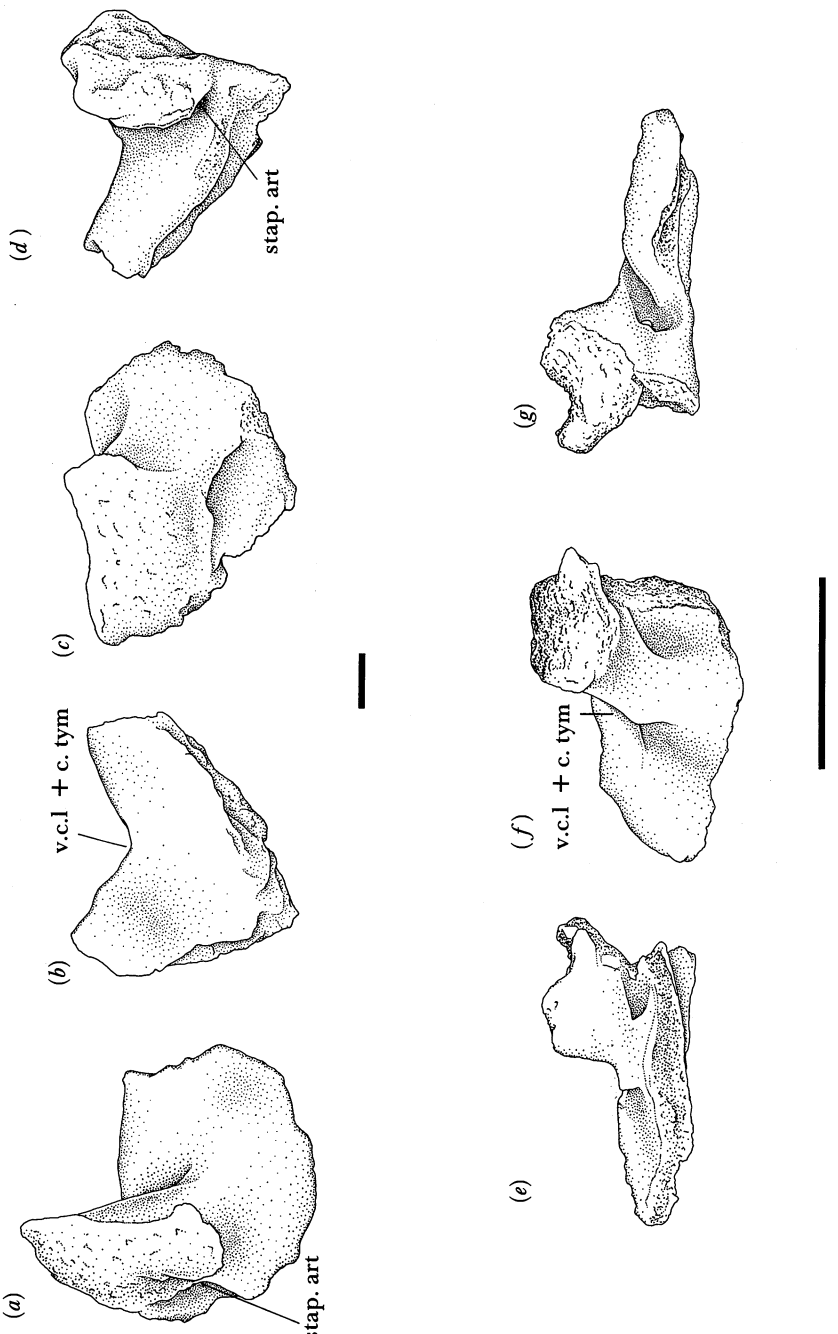

FIGURE 7. *Greererpeton burkemorani* Romer. (*a–d*) The smallest stapes known, CMNH 11320 (right). (*a*) Dorsal view; (*b*) posterior view; (*c*) mesial view; (*d*) anterior view. Scale bar 1 mm. (*e–g*) The left stapes of CMNH 11231 showing a deep furrow that may have held the vena capitis lateralis and the ramus mandibularis of the facial nerve (VII). (*e*) Posterolateral view in the plane of the distal flattened plate; (*f*) dorsomesial view perpendicular to the distal flattened plate; (*g*) anteromesial view in the plane of the distal flattened plate. Scale bar 1 cm.

PHILOSOPHICAL TRANSACTIONS OF THE ROYAL SOCIETY B BIOLOGICAL SCIENCES

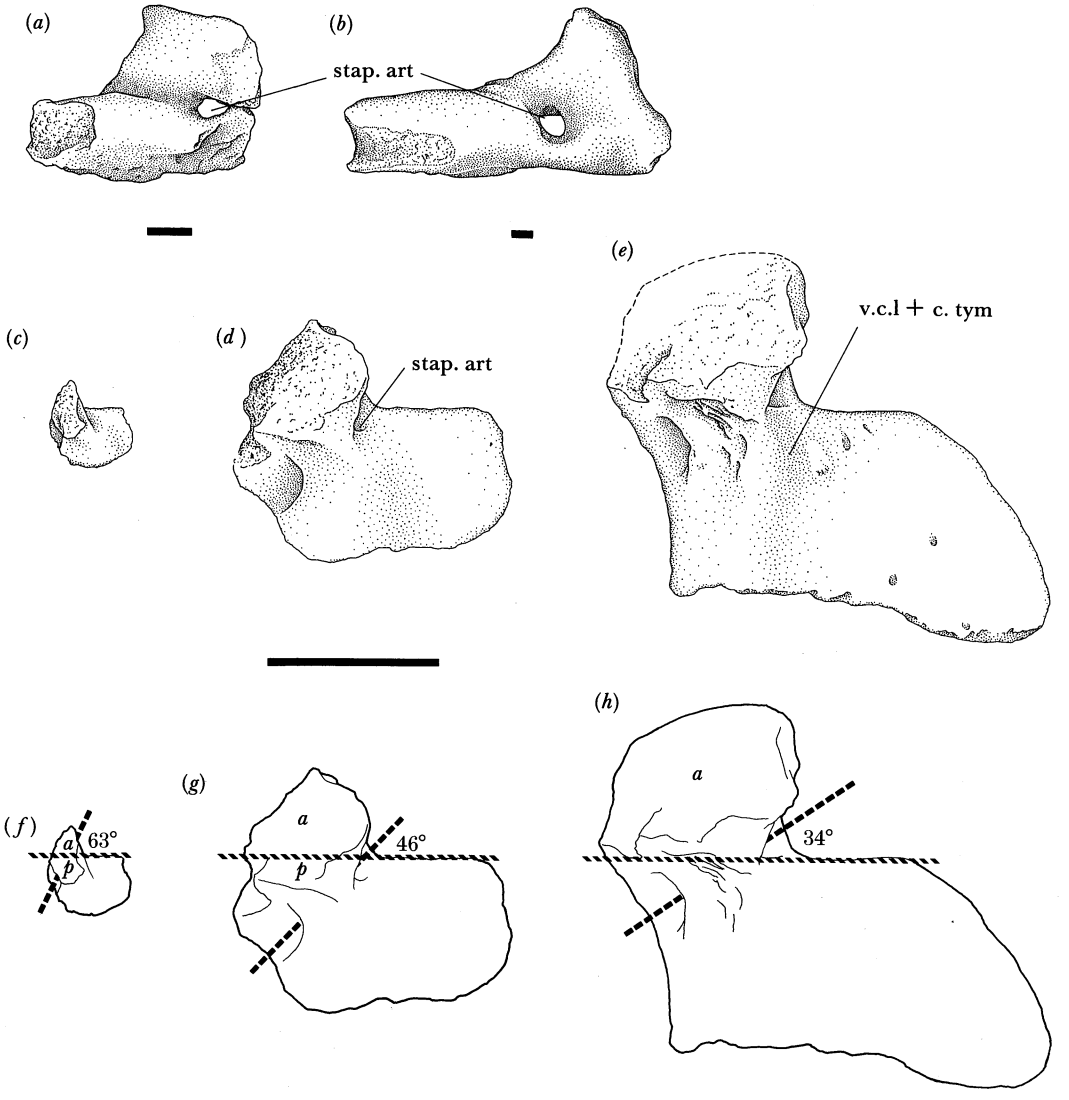

FIGURE 8. *Greererpeton burkemorani* Romer. (*a*, *b*) The position of the stapedial foramen in the right stapes as seen in an antero-laterodorsal view in (*a*) CMNH 11320 and (*b*) CMNH 11130 (an adult). Scale bars 1 mm. (*c–h*) Proportional changes to the stapes during ontogeny (viewed perpendicular to the distal flattened plate). (*c*, *f*) CMNH 11320; (*d*, *g*) CMNH 11130; (*e*, *h*) CMNH 11319. (*f–h*) The angles are formed by one line running through the stapedial foramen and the other running parallel to the anterior margin of the distal flattened plate. Scale bar 1 cm.

increase in the length of *a* (CMNH 11130) with a concomitant decrease in the relative length of *p*, such that in the very largest stapes of *G. burkemorani* known (CMNH 11319), the entire stapedial head lies anterior to the aforementioned reference line. Additional ossification of the stapedial head resulted in a conspicuous shift in the orientation of the head relative to the distal flattened plate. From the condition seen in CMNH 11320, where there is little or no exposure of the unfinished stapedial head anteriorly, ossification proceeded until the stapedial head was directed almost entirely anteriorly in CMNH 11319.

The second trend is a progressive decrease in the angle formed by a line running through the stapedial foramen and that lying along the anterior margin of the distal flattened plate. In

CMNH 11320, the angle formed between these two lines is approximately 63°, in CMNH 11130 the angle is only about 46°; whereas in CMNH 11319 it has decreased to 34°. Even though the stapedial head grew anteromesially, the element appears to have experienced more intensive growth mesiolaterally. In CMNH 11320, the distal flattened plate of the stapes, which abuts against the quadrate ramus of the pterygoid, is essentially square in outline and not nearly as elongate mesiolaterally as in mature individuals. This trend appears to be confirmed by principal-component analysis. With an eigenvector coefficient of 0.580 (table 1*c*), the mesiolateral width of the stapes increased at a faster rate than did its anteroposterior length (0.453). The anterior margin of this plate in CMNH 11320 is rounded and finished with smooth periosteal bone, whereas its lateral and posterior margins are unfinished surfaces that were continued by cartilage in life.

Until now only intrinsic modifications to the stapes have been considered. When the eigenvector coefficients between the stapes and other cranial parameters are examined (table 1*c*) the former load conspicuously higher. The mesiolateral width of the stapes increased at a much faster rate than did the length of the skull. When measured relative to the length of the braincase, which decreased in length with respect to the length of the skull table, the difference between the coefficient loadings is even greater.

Discussion

As in most other vertebrates, the predominance of isometric growth throughout the skull of *G. burkemorani* enables recognition of a juvenile of this taxon. A proportional decrease in the diameter of the orbit in *G. burkemorani* is not unexpected, as negative allometry of the orbital diameter is one of the most conspicuous changes observed in vertebrate skulls during ontogeny (Dodson 1975*b*). In a study of ontogenetic changes in the osteolepiform fish *Eusthenopteron foordi*, Schultze (1984) noted that positive allometry of the circumorbital bones (posterior tectal, supraorbital, postorbital, jugal, and lacrimal) resulted in negative allometry of the orbit diameter. Unlike *G. burkemorani*, positive allometry of the dermal bones between the orbits in *E. foordi* shifted the dorsomesial rim of each orbit laterally (Schultze 1984).

In both *E. foordi* and *G. burkemorani*, the snout appears to have experienced positive allometric growth over the intervals studied. Allometric elongation of the snout relative to skull length does not in fact occur. Rather it is an illusion created by the large allometric decrease in the diameter of the orbit. Holmes (1984) found no evidence for an allometric increase in the length of the snout in a small growth series (four specimens) of the anthracosaur *Proterogyrinus scheelei*. Stability in the relative position of the orbits in *G. burkemorani* is not shared by all early tetrapods. Panchen (1970) proposed that if the British eogyrinids form an allometric series, larger taxa would exhibit a higher growth rate in the antorbital region as compared to their postorbital region. In *Benthosuchus sushkini*, the orbits migrated posteriorly as the snout became proportionately longer during ontogeny (Bystrow & Efremov 1940).

In *Branchiosaurus credneri*, Watson (1963) noted that the pineal foramen migrated relatively further back on the skull table during ontogeny. As in *E. foordi*, relative movement in the position of the pineal foramen does not appear to occur in *G. burkemorani* over the size range represented by the known specimens.

Negative allometry of the vertebrate braincase is not uncommon during ontogeny (Watson 1963; Dodson 1975*b*). Proportional changes in the braincase of *G. burkemorani* appear to have

had a major influence on the configuration of the stapes. The bulk of allometric changes in the stapes may be accounted for by at least two major factors. The first, and most obvious, is the lack of ossification of this ossicle in immature individuals. The magnitude of the component loading may be partly artificial because there probably were extensive cartilaginous portions of the juvenile stapes that are not preserved. Proportional changes in the configuration of the stapes are probably a reflection of the role played by this ossicle as a brace for the back of the braincase (Carroll 1980; Smithson 1982). Although the stapes may have transmitted vibrations from the quadrate ramus of the pterygoid to the otic capsule, its primary (?) role appears to have been one of mechanical support; preventing the braincase from being pulled, by hypaxial muscular contraction, away from its relatively feeble osseous moorings beneath the dermal skull roof (Smithson 1982). As the skull grew longer during ontogeny, the length of the braincase did not keep pace. At the same time, the width of the back of the skull table increased at a faster rate than did overall skull length. As the proportions of the braincase and skull table changed during ontogeny, so too did the configuration of the stapes for it to act in its capacity as the principal element supporting the back of the braincase. Allometric changes in the distance between the quadrates and the quadrate rami of the pterygoids on contralateral sides of the skull may have played a part in the large allometric changes observed in the stapes. Unfortunately, mesial or lateral deflection of the suspensorium *post mortem*, in most skulls of *G. burkemorani*, precluded satisfactory measurement of the distance between the quadrates.

I thank Dr R. L. Carroll, under whose guidance this project was undertaken. I am indebted to Dr M. Williams and the Cleveland Museum of Natural History for their permission to study *G. burkemorani*. Collection and initial preparation of the material was done by the staff of the Cleveland Museum, supported by the United States National Science Foundation, grant G.B.-35474. Dr F. Jenkins and Mr C. Schaff of the Museum of Comparative Zoology, Harvard University and Dr N. Hotton III of the United States National Museum, are thanked for providing access to the specimens of *G. burkemorani* in their care.

I also thank Dr P. Jolicoeur (Université de Montreal) and Dr K. Somers (University of Toronto) for their comments on the principal-component analyses. Editorial comments by Dr R. L. Carroll, Dr R. Holmes, Dr B. Hook, Dr D. Walsh, Ms C. Wright and two anonymous reviewers substantially improved the quality of this paper.

This research was supported by the Natural Sciences and Engineering Research Council of Canada and McGill University.

PHILOSOPHICAL TRANSACTIONS OF THE ROYAL SOCIETY B BIOLOGICAL SCIENCES

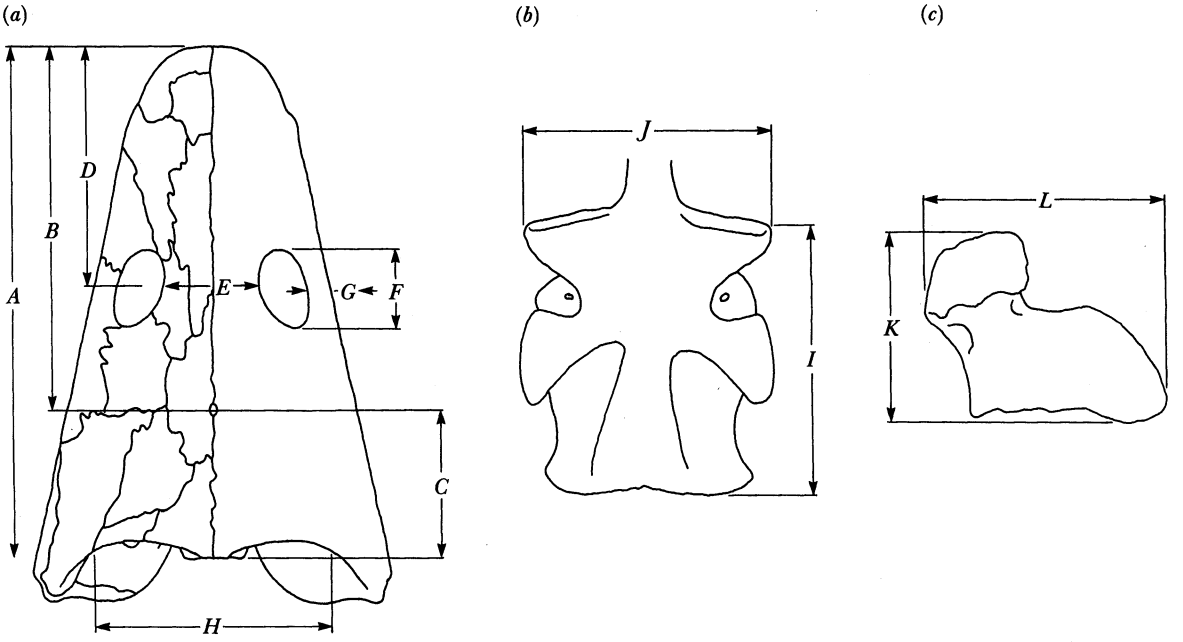

FIGURE A 1. *Greererpeton burkemorani* Romer. Outline drawings of (*a*) the dermal skull roof in dorsal view; (*b*) the otico-occipital moiety of the braincase in ventral view; and (*c*) the stapes viewed perpendicular to the plane of the distal flattened plate. The lettered dimensions (*A–L*) correspond to those listed below. Drawings are not to scale.

APPENDIX 1. CRANIAL DIMENSIONS OF *GREERERPETON BURKEMORANI* ROMER, 1969

(All measurements in millimetres.)

											K		L	
CMNH	*A*	*B*	*C*	*D*	*E*	*F*	*G*	*H*	*I*	*J*	left	right	left	right
10931§	(146)†	(108)	(38)	(65)	(28)	23	(15)	(70)	26	24	—‡	—	—	—
11034	154	—	—	74	—	—	—	68	(27)	(21)	—	—	—	—
11036§	140	101	39	67	25	(20)	16	70	26	20	—	—	—	—
11068§	170	123	47	81	14	26	16	84	32	27	—	13	23†	23.5
11069§	127	91	36	60	21	18	10	58	25	19	8	8	14	(13)
11072§	150	(107)	43	(72)	30	(22)	13	(74)	—	—	—	—	—	—
11073§	148	105	43	73	(25)	(20)	15	77	—	—	—	—	—	—
11079§	155	110	45	74	26	23	14	(70)	29	24	—	—	—	—
11082	123	89	34	60	(23)	(20)	12	64	—	—	—	—	—	—
11090§	140	101	39	62	25	19	14	66	28	22	9	11	18.5	(18)
11093§	130	93	37	61	25	20	13	66	26	19	—	9	—	15.5
11095§	—	28	—	18	7	8	1	—	—	—	—	—	—	—
11113§	—	—	28	—	(22)	14	8	45	—	—	—	—	—	—
11130§	(124)	(87)	(37)	55	23	20	12	(68)	25	(21)	7.5	8.5	15	16.5
11131	129	93	36	(67)	26	20	10	62	—	—	—	—	—	—
11132§	(142)	100	40	64	27	20	13	76	23	(20)	—	10	(20)	17.5
11219§	154	110	44	72	23	21	15	(64)	—	—	—	—	—	—
11220§	153	112	41	73	25	23	13	(71)	—	25	—	11.5	—	21
11231§	—	—	33	—	—	—	—	52	(25)	(20)	(7)	—	14.5	—
11234	—	—	—	—	—	—	14	—	(29)	(25)	—	—	—	—
11240	—	—	—	—	—	—	—	—	—	—	14	—	23.5	—
11319§	(162)	(110)	47	78	—	—	(17)	87	31	28	13.5	13.5	25	25.5
11320§	(73)	(52)	21	(36)	13	14	5	28	16	10	3.5	3.5	4.5	5
11073(2)§	(103)	(71)	(32)	53	—	—	10	(50)	23	20	7.5	—	—	—
USNM 22576§	140	101	39	69	27	—	—	—	—	—	—	—	—	—

† Brackets indicate measurement uncertain.
‡ Dash indicates measurement missing or obscured.
§ Skull used in the PGA.

PHILOSOPHICAL TRANSACTIONS OF THE ROYAL SOCIETY B BIOLOGICAL SCIENCES

References

Bernacsek, G. M. & Carroll, R. L. 1981 Semicircular canal size in fossil fishes and amphibians. *Can. J. Earth* **18**, 150–156.

Blackith, R. E. & Reyment, R. A. 1971 *Multivariate morphometrics*. London and New York: Academic Press.

Bystrow, A. P. & Efremov, J. A. 1940 *Benthosuchus sushkini* Efremov – a labyrinthodont from the Eotriassic of Sharjenga River. *Trudȳ paleont. Inst.* **10**, 1–152.

Carroll, R. L. 1980 The hyomandibular as a supporting element in the skull of primitive tetrapods. In *The terrestrial environment and the origin of land vertebrates*, Systematics Association special volume no. 15 (ed. A. L. Panchen), pp. 293–317. London: Academic Press.

Chatfield, C. & Collins, A. J. 1980 *Introduction to multivariate analysis*. London and New York: Chapman and Hall.

de Beer, G. R. 1937 *The development of the vertebrate skull*. London: Clarendon Press.

Dodson, P. 1975*a* Functional and ecological significance of relative growth in *Alligator*. *J. Zool.* **175**, 315–355.

Dodson, P. 1975*b* Relative growth in two sympatric species of *Sceloporus*. *Am. Midl. Nat.* **94** (2), 421–450.

Godfrey, S. J. 1988 Isolated tetrapod remains from the Carboniferous of West Virginia. *Kirtlandia* **43**, 27–36.

Godfrey, S. J. 1989 The postcranial skeletal anatomy of the Carboniferous tetrapod *Greererpeton burkemorani* Romer, 1969. *Phil. Trans. R. Soc. Lond.* B **323**, 75–133.

Gould, S. J. 1975 Allometry in primates, with emphasis on scaling and the evolution of the brain. In *Approaches to primate paleobiology* (ed. H. Kuhn *et al.*). *Contrib. Primatol.* **5**, 244–292.

Gould, S. J. 1981 *The mismeasure of man*. New York and London: W. W. Norton.

Holmes, R. 1984 The Carboniferous amphibian *Proterogyrinus scheelei* Romer, and the early evolution of tetrapods. *Phil. Trans. R. Soc. Lond.* B **306**, 431–527.

Jolicoeur, P. 1963 The multivariate generalization of the allometric equation. *Biometric* **19**, 497–499.

Jolicoeur, P. & Mosimann, J. E. 1960 Size and shape variation in the painted turtle. A principal component analysis. *Growth* **24**, 339–354.

Panchen, A. L. 1970 Teil 5a: Anthracosauria. *Handbuch der Palaoherpetologie* (ed. O. Kuhn), pp. 1–84. Stuttgart: Fischer.

Romer, A. S. 1930 The Pennsylvanian tetrapods of Linton, Ohio. *Bull. Am. Mus. nat. Hist.* **59**, 77–147.

Romer, A. S. & Witter, R. V. 1942 *Edops*, a primitive rhachitomous amphibian from the Texas red beds. *J. Geol.* **50**, 925–960.

SAS Institute 1982 *SAS user's guide*: *basics*. Cary, N.C: SAS Institute.

Sawin, H. J. 1941 The cranial anatomy of *Eryops megacephalus*. *Bull. Mus. Comp. Zool. Harv. Univ.* **88**, 407–463.

Shishkin, M. A. 1968 On the cranial arterial system of the labyrinthodonts. *Acta zool., Stockh.* **49**, 1–22.

Schultze, H.-P. 1984 Juvenile specimens of *Eusthenopteron foordi* Whiteaves, 1881 (Osteolepiform Rhipidistian, Pisces) from the late Devonian of Miguasha, Quebec, Canada. *J. Vertebr. Paleont.* **4** (1), 1–16.

Smithson, T. R. 1982 The cranial morphology of *Greererpeton burkemorani* Romer (Amphibia: Temnospondyli). *Zool. J. Linn. Soc.* **76**, 29–90.

Watson, D. M. S. 1963 On growth stages in branchiosaurs. *Palaeontology* **6**, 540–553.

Abbreviations used in the figures

ang	angular
a.p.f.	anterior palatal fenestra
b.p	basal process of the pterygoid/epipterygoid
basi	basioccipital
bas. p	basipterygoid process
c. tym	groove or notch for the chorda tympani
clav	clavicle
cr. vent	crista ventrolateralis
d	dentary
d. n	dentary notch
ect	ectopterygoid
f	frontal
f. mag	foramen magnum
f. pa	facet for the proatlas on the exoccipital
j	jugal
l	lacrimal
m	maxilla
n	nasal
p	parietal
pa	parasphenoid
pal	palatine
po	postorbital
pf	postfrontal
pp	postparietal
prf	prefrontal
prm	premaxilla
prsp	presplenial
psp	postsplenial
pt	pterygoid
sq	squamosal
st	supratemporal
stap	stapes
stap. art	foramen for the stapedial artery
sur	surangular
t	tabular
tub. bas	'tubera basisphenoidales'
v	vomer
v.c.l	groove or notch for the vena capitis lateralis
VII	foramen for cranial nerve VII
X	foramen for cranial nerve X
XII	foramen for cranial nerve XII

PHILOSOPHICAL TRANSACTIONS OF THE ROYAL SOCIETY B BIOLOGICAL SCIENCES